



Photocatalytic hydrogen evolution systems constructed in cross-linked porous protein crystals



Hiroyasu Tabe^a, Hikaru Takahashi^a, Takuya Shimoi^b, Satoshi Abe^b, Takafumi Ueno^{b,*}, Yusuke Yamada^{a,*}

^a Department of Applied Chemistry and Bioengineering, Graduate School of Engineering, Osaka City University, Osaka 558-8585, Japan

^b School of Life Science and Technology, Tokyo Institute of Technology, 4259-B55, Nagatsuta-cho, Midori-ku, Yokohama 226-8501, Japan

ARTICLE INFO

Keywords:

Heterogeneous catalysis
Photocatalysis
Hydrogen evolution
Protein crystal
Lysozyme

ABSTRACT

Cross-linked hen egg white lysozyme crystals (CL-HEWL) have been employed as supports to construct heterogeneous catalysts for photocatalytic hydrogen (H_2) evolution, where rose bengal (RB) and Pt nanoparticles (PtNPs) acted as a photosensitizer and H_2 -evolution catalysts, respectively. Single-crystal X-ray structure analyses of the CL-HEWL immobilizing a precursor for PtNPs suggested that a coordination site of the precursor locates in immediate proximity to potential adsorption sites for RB. The accumulation of the components facilitated photo-induced electron transfer, resulting in efficient H_2 evolution. These results suggest that porous protein crystals are promising platforms to periodically and rationally accumulate catalytic components by using molecular interactions.

1. Introduction

Bio-supramolecular structures utilizing proteins have attracted much attention to develop highly sophisticated functional materials [1–10], because multiple functional molecules can be immobilized simultaneously in a protein crystal by utilizing specific interaction with the functional groups of amino acids [11,12]. Additionally, interaction of side chains among proteins often induces self-assembled nanostructures available as nano-vessels for immobilization of metal clusters composed of multiple atoms [13–16]. Moreover, metal nanoparticles larger than the metal clusters can be immobilized in protein crystals where larger spaces are available among protein molecules aligned periodically [17–19]. Recently, protein crystals with a cross-link treatment have emerged as a robust porous material [20]. The pores can be provided by removal of solvent molecules from, so-called, solvent channels, in which metal complexes and organic compounds can be immobilized by selective interactions such as coordination, electrostatic interaction, hydrophobic interaction, etc, with the functional groups at the pore walls [21–24]. In fact, site-selective immobilization of metal nanoparticles by reduction of pre-organized metal complexes in solvent channels has been reported [14], indicating that sophisticated functional materials can be achieved by cooperative immobilization of functional molecules and metal nanoparticles in porous protein crystals.

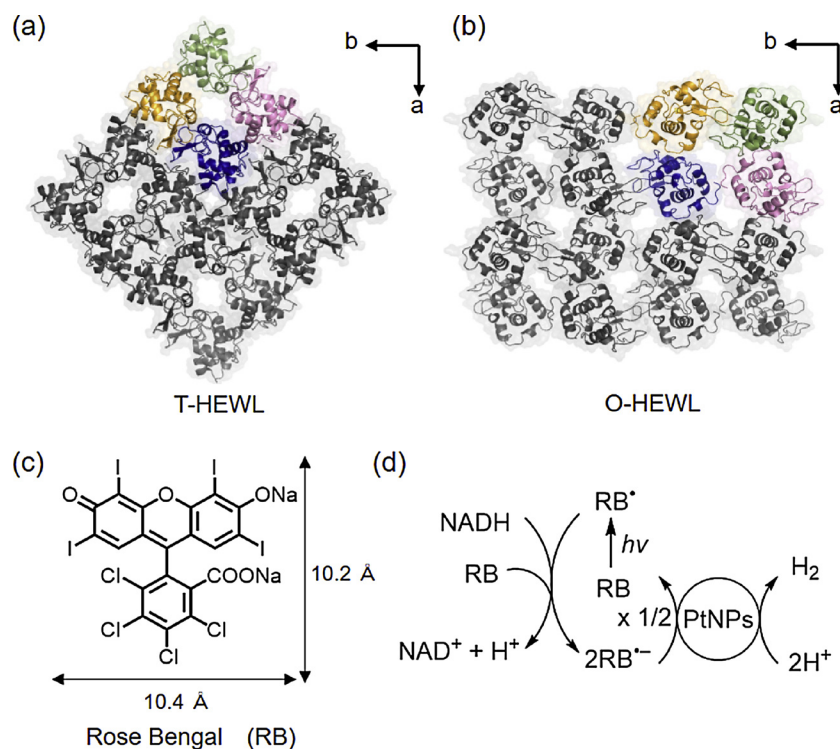
Cooperative immobilization of a photoresponsible molecule and

metal nanoparticles can provide solar energy conversion systems to produce high-energy compounds such as hydrogen (H_2) [25–28]. Efficient photocatalytic H_2 -evolution systems can be achieved by combination of several catalytic components including light-harvesting and charge-separation units and water-oxidation and reduction catalysts developed separately [29–38]. These components are usually combined in an appropriate solvent, however, back electron transfer between oxidation and reduction catalysts is hardly avoidable. Immobilization of these components with arrangement suitable for forward electron transfer can enhance the photocatalytic efficiency on the surfaces of a solid support such as mesoporous silica-alumina [34–38]. However, amorphous nature of mesoporous silica-alumina disturbs precise and periodical arrangement of components, which is necessary for efficient photocatalytic H_2 evolution. In addition, anionic components are hardly immobilized on silica-alumina due to the electrostatic repulsion.

We report herein photocatalytic H_2 -evolution systems constructed in cross-linked hen egg white lysozyme crystals by immobilizing Pt nanoparticles (PtNPs) as H_2 -evolution catalysts in immediate proximity to an anionic photosensitizer molecule, rose bengal (RB). β -Dihydronicotinamide adenine dinucleotide (NADH) was employed as an electron donor, because irreversibly decomposing nature of NADH during the reaction can result in quantitative H_2 evolution, allowing to evaluate the efficiency of the reaction systems by H_2 yields [39]. Construction of photocatalytic H_2 evolution systems composed of molecular H_2 -evolution catalyst and molecular photosensitizers in a viral

* Corresponding authors.

E-mail addresses: ueno@bio.titech.ac.jp (T. Ueno), ymd@chem.eng.osaka-cu.ac.jp (Y. Yamada).



Scheme 1. Porous structure of HEWL crystals in (a) tetragonal form (T-HEWL) and (b) orthorhombic form (O-HEWL) from the Protein Data Bank (PDB), codes: 193L and 1BGI, respectively. (c) Chemical structure of rose bengal (RB) and (d) the overall photocatalytic cycle of H_2 evolution.

protein particle has been reported [7], however, the small interior space allowed no co-immobilization of metal nanoparticles and photosensitizers. Larger inner spaces of porous protein crystals are necessary for co-immobilization of an organic photosensitizer and metal nanoparticles. Additionally, porous protein crystals immobilizing exogenous molecules are stable in a photoreaction under visible light irradiation [40]. Thus, cross-linked hen egg white lysozyme crystals in the tetragonal form (CL-T-HEWL) and in the orthorhombic form (CL-O-HEWL) were employed as porous supports (Scheme 1a and b). The prepared catalysts were characterized by single-crystal X-ray structure analyses and TEM observations. Photocatalytic H_2 evolution was performed in the presence of NADH under visible-light irradiation of a suspension containing the composite photocatalysts. The chemical structure of RB and the overall photocatalytic cycle are indicated in Scheme 1c and d, respectively. The accumulation of the components resulted in increasing the amount of evolved H_2 to three times that of a homogeneous system without the HEWL crystals.

2. Experimental section

2.1. Materials

Hen egg white lysozyme (HEWL) was purchased from Sigma-Aldrich Co. LLC. Other reagents were purchased from Tokyo Chemical Industry Co., Ltd. and Wako Pure Chemical Industries, Ltd., and were used without further purification.

2.2. Catalyst characterization

UV-vis absorption spectra of rose bengal (RB) on each CL-T-HEWL composite were measured using a JASCO V-770 with an integrating sphere attachment. The atomic ratio of sulfur, iodine and platinum in each CL-T-HEWL composite was determined using a Shimadzu EDX-730 X-ray fluorescence spectrometer. Transmission electron microscope (TEM) images of PtNP@RB-CL-T-HEWL were obtained using a

JEOL JEM-2100 equipped with a field-emission gun with an accelerating voltage of 200 kV. Thin pieces of PtNP@RB-CL-T-HEWL were fixed on a Cu-mesh microgrid coated with an amorphous carbon supporting film.

2.2.1. Single-crystal X-ray structure analysis

The hanging drop vapor diffusion method was used to obtain HEWL crystals in the tetragonal form and in the orthorhombic form followed by the cross-linking treatment (CL-T-HEWL and CL-O-HEWL, respectively) [41,42]. These crystals were soaked in a drop of HEPES buffer (10 mM, pH 7.8) containing RB (10 mM) and NaCl (1.0 M) at room temperature for 24 h (RB-CL-T-HEWL and RB-CL-O-HEWL, respectively) followed by soaking in a drop of HEPES buffer (10 mM, pH 7.8) containing $H_2PtCl_6 \cdot 6H_2O$ (10 mM) and NaCl (1.0 M) for 24 h. Although we attempted to soak crystals in buffer solution containing RB more than 10 mM, the crystals cracked during the incubation. Prior to data collection, crystals were continuously immersed in the precipitant solutions containing 10% and 25% (w/w) glycerol and subsequently frozen in liquid nitrogen. X-ray diffraction datasets for the sample were collected at 100 K at beamline BL26B1 at SPring-8 using X-ray wavelengths of 1.0 Å. The data were processed with the program HKL2000 [43].

The crystal parameters and the data collection statistics are summarized in Table S2. The structures were solved by molecular replacement with MOLREP [44] by using tetragonal and orthorhombic HEWL structures (PDB ID: 193L and 1BGI, respectively). Refinement of the protein structures was performed using REFMAC5 [45] in the CCP4 suite [46]. Rebuilding was performed using COOT [47] based on sigma-weighted ($2F_o - F_c$) and ($F_o - F_c$) electron density maps. After rigid-body refinement, the coordination structures of Pt binding sites were determined using anomalous Fourier difference maps and geometric parameters. Water molecules were positioned to fit residual ($F_o - F_c$) density peaks with a lower cut-off of 3σ . The models were subjected to quality analysis during the various refinement stages with omit maps and RAMPAGE [48]. The refinement statistics are summarized in Table S1. Atomic coordinates for RB-CL-T-HEWL composite are deposited in

the Protein Data Bank under accession number: 5YKY.

2.3. Preparation of the composite of CL-X-HEWL (X = T, O) with RB (RB-CL-X-HEWL)

HEWL crystals in the tetragonal form were obtained using a batch crystallization method followed by a cross-linking treatment according to the previously reported procedure (CL-T-HEWL) [41]. CL-T-HEWL (100 mg) was soaked in HEPES buffer (10 mM, pH 7.8, 50 mL) containing rose bengal (RB, 1.0 mM) at room temperature for 12 h to immobilize RB in CL-T-HEWL. The composite of CL-T-HEWL with RB was obtained as dark red crystals (RB-CL-T-HEWL). The same procedure was applied to obtain the composite of cross-linked orthorhombic HEWL crystals with RB (RB-CL-O-HEWL) [42].

2.4. Photocatalytic hydrogen evolution by the composite of RB-CL-T-HEWL with Pt nanoparticles via a photodeposition method

A phosphate buffer suspension (50 mM, pH 8.0, 2.0 mL) containing RB-CL-T-HEWL (2.5 mg), β -dihydronicotinamide adenine dinucleotide (NADH, 10 mM) and $H_2PtCl_6 \cdot 6H_2O$ (0.097 mM) was flushed with N_2 gas for 40 min. The suspension was then photoirradiated for a certain time using a white LED light (130 mW, 33.2 mW cm^{-2} , RelyOn Ltd., Japan) positioned perpendicular to a cuvette at a distance of 3.0 cm. While photoirradiation, RB-CL-T-HEWL gradually turned to black to form Pt nanoparticles (PtNPs) inside RB-CL-T-HEWL (PtNP@RB-CL-T-HEWL). Gas in a headspace was analyzed by Shimadzu GC-14B gas chromatography (detector: TCD, column temperature: 80 °C, column: active carbon with the particle size 60–80 mesh, carrier gas: N_2) to determine the amount of evolved H_2 . After the H_2 evolution reaction, buffer solution containing NADH (200 mM, 100 μ L) was added to the cuvette for the next run to evaluate recycling performance of PtNP@RB-CL-T-HEWL.

2.5. Preparation of the composite of CL-T-HEWL with RB and Pt nanoparticles by a chemical reduction method

RB-CL-T-HEWL (50 mg) was soaked in an acetate buffer solution (100 mM, pH 8.0, 5.0 mL) containing $H_2PtCl_6 \cdot 6H_2O$ (2.0 mM) for 30 min, and then washed with water to remove unbound Pt complexes. CL-T-HEWL containing Pt complexes were soaked in an acetate buffer (100 mM, pH 4.8, 3.0 mL) containing $NaBH_4$ (250 mM) for 15 min, then washed with water, and dried in *vacuo* (PtNP@RB-CL-T-HEWL(CR)).

3. Results and discussion

3.1. Preparation and catalysis of composite photocatalysts

RB was immobilized in CL-T-HEWL (RB-CL-T-HEWL) by the equilibrium adsorption [49]. The diffuse reflectance UV-vis absorption spectrum of RB-CL-T-HEWL evidenced absorption of RB (Fig. S1). The amount of adsorbed RB per unit cell of CL-T-HEWL was determined to be 0.64 based on the absorbance change at 548 nm of the RB mother liquor induced by the adding CL-T-HEWL (Fig. S2). This amount is comparable to that determined by X-ray fluorescence (XRF) spectroscopy based on the molar ratio of iodine in RB and sulfur in CL-T-HEWL (0.45, Table S1).

RB-CL-T-HEWL was soaked in a buffer solution containing H_2PtCl_6 (10 mM) as the precursor for Pt nanoparticles. The crystal structure of soaked RB-CL-T-HEWL was determined at 1.88 Å resolution (PDB ID: 5YKY; Fig. 1a, b and Table S2). Two positions for immobilizing the Pt complexes were determined by the anomalous difference maps. A Pt complex at a Pt_a position is bound to N^e of His15 with the Pt_a-N^e length of 2.5 Å, as reported for HEWL crystals with other Pt-halide complexes (Fig. 1c) [50,51]. Five Cl^- ions bound to the Pt_a ion fulfill the octahedral coordination. The other Pt complex in the form of $[Pt_bCl_6]^{2-}$ was

immobilized in the anion exchange site by the positively charged side chain of Lys1 by electrostatic interaction where the distance between Pt_b and N^a of Lys1 was 3.4 Å (Fig. 1d) [50]. Although unambiguous positions of RB were hardly determined, negatively charged RB is expected to be immobilized with positively charged side chains of Arg5, Arg125 and Arg21 from an adjacent HEWL monomer in the solvent channel (Figs. 1b and S3). The distance between a binding site for a Pt complex and the positively charged areas is enough close for electron transfer (*ca.* 2 nm). Pt complexes were converted into PtNPs by the reduction with photogenerated $RB \cdot^-$ followed by the photocatalytic reaction, because metal nanoparticles are grown in the region where pre-organized metal complexes are bound as reported previously [14].

Photocatalytic H_2 evolution was performed by the photoirradiation of a phosphate buffer dispersion (pH 8.0) containing RB-CL-T-HEWL (2.5 mg), H_2PtCl_6 (0.097 mM) and NADH (10 mM) as an electron donor as shown in Fig. 2 (solid line). PtNP@RB-CL-T-HEWL exhibited the activity for photocatalytic H_2 evolution with the initial H_2 -evolution rate of 0.73 μ mol h^{-1} and the H_2 yield of 17 μ mol for 24 h, suggesting that a photocatalytic system was successfully constructed in CL-T-HEWL. The H_2 yield based on the used amount of NADH reached 85%, where the turnover frequency (TOF) of evolved H_2 per RB was 13 h^{-1} . The H_2 yield was higher than that (76%) reported for a photocatalytic H_2 -evolution system using an assembly of monodispersed silica-alumina nanoparticles as a porous support together with 2-phenyl-4-(1-naphthyl)quinolinium cation, PtNPs and NADH as a photosensitizer, an H_2 -evolution catalyst and an electron donor, respectively [36]. Moreover, the TOF was increased from those of catalytic systems constructed using a spherical mesoporous silica-alumina (0.9 h^{-1}) or a porous assembly of monodispersed silica-alumina nanoparticles (4.6 h^{-1}) as supports [36–38].

A homogeneous reaction system using a buffer solution containing PtNPs, RB and NADH without RB-CL-T-HEWL, which is similar to the method described in the previous report, resulted in lower H_2 yield (5.3 μ mol, 27%, for 6 h) than that with PtNP@RB-CL-T-HEWL although the initial H_2 -evolution rate is relatively high (0.97 μ mol h^{-1} , Fig. 2, dashed line) [53]. The mixture of PtNPs, RB, NADH and CL-HEWL in a buffer solution also showed the low activity for H_2 evolution (2 μ mol, 11%, for 23 h, Fig. 2, the dashed double-dotted line) compared with PtNP@RB-CL-T-HEWL. These results suggest that the immobilization of each component in a solvent channel of HEWL crystals enhanced the stability of the catalytic system. Slightly slower H_2 evolution with CL-T-HEWL can be explained by slow diffusion of NADH in the solvent channels. The amounts of RB and Pt per HEWL monomer for PtNP@RB-CL-T-HEWL determined by XRF were 0.035 and 0.036, respectively (Table S1). Formation and growth of PtNPs during the reaction were confirmed by a transmission electron microscope (TEM). PtNPs in the size of *ca.* 1 nm (Fig. S5a) on RB-CL-T-HEWL were observed soon after the induction period (*~*5 h). Growing PtNPs with the size of *ca.* 2 nm were observed at the prolonged reaction time of 24 h (Fig. S5b). Formed PtNPs were well-dispersed throughout the crystals of RB-CL-T-HEWL and smaller than the size of solvent channels of CL-T-HEWL.

RB-CL-O-HEWL with PtNPs (PtNP@RB-CL-O-HEWL) also showed the activity for photocatalytic H_2 evolution (Fig. 2, dotted dashed line). Single-crystal X-ray structure analysis of RB-CL-O-HEWL indicated that electron density originated from a Pt ion was found at the Pt_a position while this density was too low to fit the models of a Pt-chloride complex (Fig. S4 and Table S2). The positively charged area around Arg5 and Arg125 from an adjacent HEWL monomer is located with separation distances of *ca.* 2 nm from Pt_a (Fig. S4). Thus, the catalytic activity of PtNP@RB-CL-O-HEWL is comparable to that of PtNP@RB-CL-T-HEWL.

CL-T-HEWL with PtNPs was also prepared by chemical reduction (CR) of Pt complexes by $NaBH_4$ according to a previously reported procedure (PtNP@RB-CL-T-HEWL(CR)) [23]. The amount of Pt per HEWL monomer determined by XRF is about 5 times higher than that of PtNP@RB-CL-T-HEWL (0.16, Table S1). However, only negligible amount of H_2 ($< 1 \mu$ mol in 12 h) was evolved with PtNP@RB-CL-T-

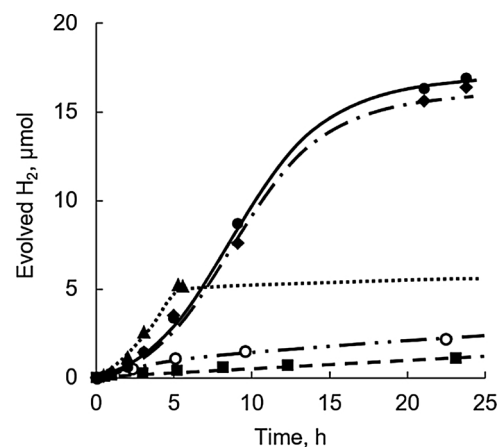
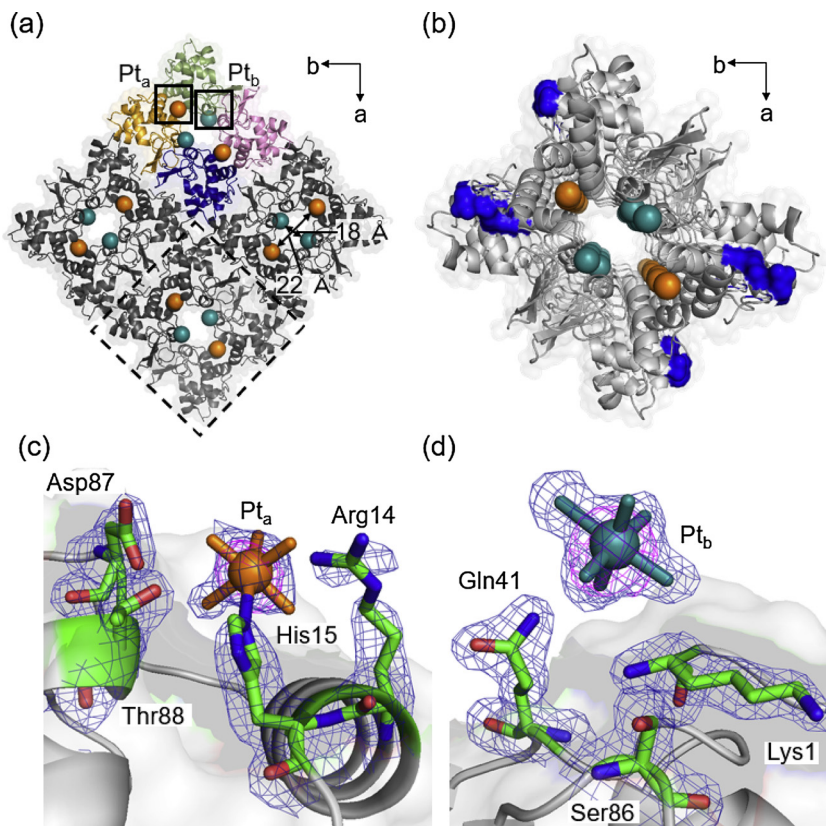


Fig. 2. Time courses of H₂ evolution under photoirradiation ($\lambda > 340$ nm) of a deaerated dispersion of a phosphate buffer (50 mM, pH 8.0, 2.0 mL) containing PtNP@RB-CL-T-HEWL (●, solid line), PtNP@RB-CL-O-HEWL (◆, dashed dotted line), PtNP@RB-CL-T-HEWL(CR) (■, dashed line), homogeneous solution of H₂PtCl₆ with RB (▲, dotted line) and the mixture of homogeneous solution of H₂PtCl₆ with RB and CL-T-HEWL (○, dashed double-dotted line), in the presence of NADH (10 mM).

HEWL(CR) (Fig. 2, dashed line). The TEM image in Fig. S5c showed that the particle size of PtNPs in PtNP@RB-CL-T-HEWL(CR) was as small as *ca.* 3 nm. As previously reported, PtNPs generated by CR originated from pre-organized Pt ions in ~10 neighboring HEWL monomers [23]. Thus, PtNPs were immobilized irrespective of the positions of adsorbed RB. On the other hand, PtNPs generated by the reduction with photo-generated RB[·] were immobilized in immediate proximity to adsorbed RB, where efficient electron transfer from photogenerated RB to PtNPs is possible.

Fig. 1. (a) The overall structure of RB-CL-T-HEWL immobilizing pre-organized Pt-chloride complexes. The Pt atoms are represented by spheres. (b) Magnifications of a pore indicated by a dashed square in (a). Blue residues indicate positively charged area on the surface of solvent channels. (c, d) Magnifications of two Pt binding sites indicated by the black squares in (a). Anomalous difference Fourier maps at 3.0 σ indicate the positions of individual Pt atoms (magenta and turquoise). Selected 2Fo–Fc electron-density maps at 1.0 σ are the deep blue mesh. Crystallographic images were produced by Pymol [52]. (For interpretation of the references to color in this figure legend, the reader is referred to the web version of this article.)

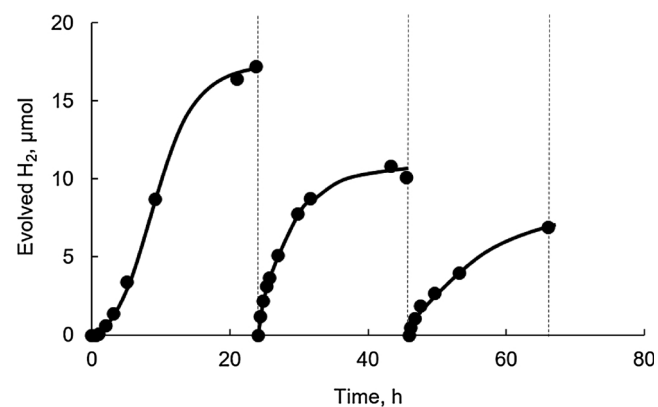


Fig. 3. Time courses of the photocatalytic H₂ evolution under photoirradiation of a deaerated phosphate buffer (50 mM, pH 8.0, 2.0 mL) containing H₂PtCl₆ (0.097 mM), RB-CL-T-HEWL (2.5 mg) and NADH (10 mM) in three repetitive experiments.

3.2. Recycling tests

The H₂ evolution lasted for more than 64 h by the successive addition of an aqueous NADH solution to the reaction solution containing PtNP@RB-CL-T-HEWL after H₂ evolution ceased (Fig. 3). The yield at each run together with the initial H₂-evolution rate was 17 μmol (85%, 0.73 μmol h⁻¹), 11 μmol (55%, 2.3 μmol h⁻¹) and 7 μmol (35%, 0.94 μmol h⁻¹), indicating that the total turnover number exceeded 5.9×10^2 . The induction period observed at the first run resulted from the PtNP formation. The RB/HEWL ratio of PtNP@RB-CL-T-HEWL determined by X-ray fluorescence spectroscopy (Table S1) decreased to 0.020 after the third run from that after the first run (0.035) due to partial leaching of RB. On the other hand, Pt/HEWL ratio after the third run (0.046) increased by 29% based on that after the first run (0.036). Thus, the spontaneous growth of PtNPs which prohibits the diffusion of

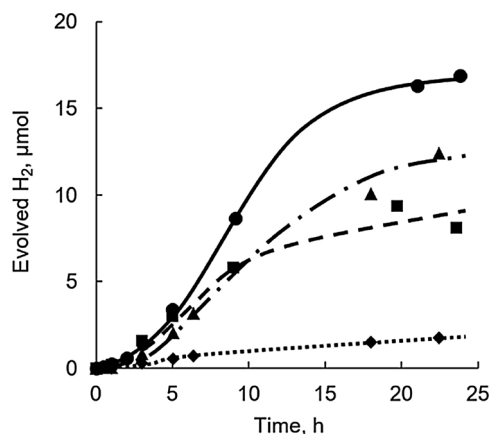


Fig. 4. Time courses of H_2 evolution under photoirradiation (white light) of a phosphate buffer (50 mM, pH 8.0, 2.0 mL) containing NADH (10 mM), RB-CL-T-HEWL (2.5 mg) and various concentrations of H_2PtCl_6 . Concentrations of H_2PtCl_6 : 0.019 mM (◆, dotted line), 0.048 mM (▲, dashed dotted line), 0.097 mM (●, solid line) and 0.72 mM (■, dashed line).

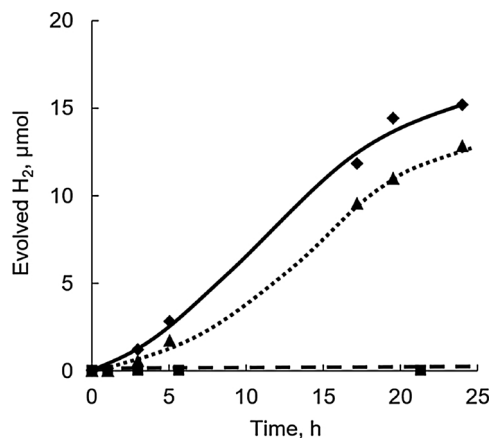


Fig. 5. Time courses of the photocatalytic H_2 evolution under photoirradiation (white light) of a deaerated phosphate buffer (50 mM, pH 8.0, 2.0 mL) containing NADH (10 mM), RB-CL-T-HEWL (2.5 mg) and various PtNP precursors (0.097 mM). A precursor of PtNPs was chosen from K_2PtCl_6 , (◆, solid line), K_2PtCl_4 , (▲, dotted line), and $\text{Pt}(\text{NH}_3)_4\text{Cl}_2$ (■, dashed line).

NADH in the solvent channels and partial leaching of RB are reasons for deceleration of H_2 evolution in repetitive runs.

3.3. Precursor effect for composite photocatalysts

The concentration effects of the Pt precursor in reaction solutions were examined ranging from 0.019 to 0.72 mM (Fig. 4). When the concentration of H_2PtCl_6 was increased to 0.72 mM from 0.097 mM, the initial reaction rate ($0.71 \mu\text{mol h}^{-1}$, Fig. 4, dashed line) is comparable to that of the original concentration although the amount of evolved H_2 was decreased to almost half ($9 \mu\text{mol}$, 45%, for 24 h) compared with that of the original concentration. This result suggests that the over-loaded H_2PtCl_6 formed larger PtNPs, which eventually prohibited the diffusion of NADH in the solvent channels. On the other hand, when the concentrations of H_2PtCl_6 were lower than 0.097 mM, the reaction rate and the amount of evolved H_2 were increased as H_2PtCl_6 increases from (Fig. 4), where no larger PtNPs formed.

Various precursor complexes for PtNPs were employed to scrutinize their effect on the catalysis. Composite catalysts prepared with K_2PtCl_6 and K_2PtCl_4 exhibited high catalytic activity, because PtCl_6^{2-} and PtCl_4^{2-} can bind to His15 and/or to the anion exchange site as reported previously (Fig. 5, solid and dotted lines) [23,54]. A composite catalyst

prepared with cationic $\text{Pt}(\text{NH}_3)_4\text{Cl}_2$ exhibited no activity for photocatalytic H_2 evolution ($< 1 \mu\text{mol}$ in 5 h, Fig. 5, dashed line), resulting from no immobilization of Pt ions in CL-T-HEWL as evidenced by XRF measurements. Strong basicity of the NH_3 ligands and electrostatic repulsion between an anion exchange site and $[\text{Pt}(\text{NH}_3)_4]^{2+}$ disturbed $[\text{Pt}(\text{NH}_3)_4]^{2+}$ from immobilization with neither histidine nor an anion exchange site.

4. Conclusion

We have successfully constructed a heterogeneous catalyst for photocatalytic H_2 evolution using cross-linked HEWL crystals as a porous support. Rose bengal was immobilized in the solvent channels of HEWL crystals and H_2 -evolution catalysts, PtNPs, were obtained from pre-organized Pt complexes in immediate proximity to rose bengal by the *in-situ* reduction of Pt complexes. The photosensitizer and the catalytic PtNPs were accumulated in the immediate proximity by utilizing coordination bonds and electrostatic interaction, resulting in efficient H_2 evolution. More sophisticated catalytic systems can be provided by employing cross-linked porous protein crystals as supports where each component can be precisely arranged by molecular interactions.

Funding sources

This work was supported by ENEOS hydrogen trust fund (to Y. Yamada); and JSPS KAKENHI [grant numbers JP16H02268 (to Y. Yamada) and JP17H07020 (to H. Tabe)].

Acknowledgements

We thank Mr. Masatsugu Ishimoto from Osaka City University for his support throughout the TEM measurements. Synchrotron radiation experiments were conducted under the approval of 2017A2718 at SPring-8 BL26B1 with the support members.

Appendix A. Supplementary data

Supplementary data associated with this article can be found, in the online version, at <https://doi.org/10.1016/j.apcatb.2018.01.046>.

References

- [1] F. Praetorius, H. Dietz, Self-assembly of genetically encoded DNA-protein hybrid nanoscale shapes, *Science* 355 (2017) eaam5488.
- [2] J.G. Heddle, S. Chakraborti, K. Iwasaki, Natural and artificial protein cages: design, structure and therapeutic applications, *Curr. Opin. Struct. Biol.* 43 (2017) 148–155.
- [3] Y. Suzuki, G. Cardone, D. Restrepo, P.D. Zavattieri, T.S. Baker, F.A. Tezcan, Self-assembly of coherently dynamic auxetic, two-dimensional protein crystals, *Nature* 533 (2016) 369–373.
- [4] J. Wang, K. Liu, R. Xing, X. Yan, Peptide self-assembly: thermodynamics and kinetics, *Chem. Soc. Rev.* 45 (2016) 5589–5604.
- [5] Q. Luo, C. Hou, Y. Bai, R. Wang, J. Liu, Protein assembly: versatile approaches to construct highly ordered nanostructures, *Chem. Rev.* 116 (2016) 13571–13632.
- [6] P.C. Jordan, D.P. Patterson, K.N. Saboda, E.J. Edwards, H.M. Miettinen, G. Basu, M.C. Thielges, T. Douglas, Self-assembling biomolecular catalysts for hydrogen production, *Nat. Chem.* 8 (2016) 179–185.
- [7] E. Edwards, R. Roychoudhury, B. Schwarz, P. Jordan, J. Lisher, M. Uchida, T. Douglas, Co-localization of catalysts within a protein cage leads to efficient photochemical NADH and/or hydrogen production, *J. Mater. Chem. B* 4 (2016) 5375–5384.
- [8] Y.T. Lai, E. Reading, G.L. Hura, K.L. Tsai, A. Laganowsky, F.J. Asturias, J.A. Tainer, C.V. Robinson, T.O. Yeates, Structure of a designed protein cage that self-assembles into a highly porous cube, *Nat. Chem.* 6 (2014) 1065–1071.
- [9] N.P. King, J.B. Bale, W. Sheffler, D.E. McNamara, S. Gonen, T. Gonen, T.O. Yeates, D. Baker, Accurate design of co-assembling multi-component protein nanomaterials, *Nature* 510 (2014) 103–108.
- [10] Y. Sano, A. Onoda, T. Hayashi, A hydrogenase model system based on the sequence of cytochrome c: photochemical hydrogen evolution in aqueous media, *Chem. Commun.* 47 (2011) 8229–8231.
- [11] J.B. Bailey, L. Zhang, J.A. Chiong, S. Ahn, F.A. Tezcan, Synthetic modularity of protein-metal-organic frameworks, *J. Am. Chem. Soc.* 139 (2017) 8160–8166.
- [12] J. Mikkila, E. Anaya-Plaza, V. Liljestrom, J.R. Caston, T. Torres, A. de la Escosura, M.A. Kostainen, Hierarchical organization of organic dyes and protein cages into

photoactive crystals, *ACS Nano* 10 (2016) 1565–1571.

[13] L. Messori, A. Merlin, Protein metallation by metal-based drugs: x-ray crystallography and mass spectrometry studies, *Chem. Commun.* 53 (2017) 11622–11633.

[14] B. Maity, S. Abe, T. Ueno, Observation of gold sub-nanocluster nucleation within a crystalline protein cage, *Nat. Commun.* 8 (2017) 14820.

[15] C. Molitor, A. Bijelic, A. Rompel, *In situ* formation of the first proteinogenically functionalized $[\text{TeW}_6\text{O}_{24}\text{O}_2(\text{Glu})]^{7-}$ structure reveals unprecedented chemical and geometrical features of the Anderson-type cluster, *Chem. Commun.* 52 (2016) 12286–12289.

[16] L. Messori, T. Marzo, R.N.F. Sanches, Hanif-Ur-Rehman, D. de Oliveira Silva, A. Merlin, Unusual structural features in the lysozyme derivative of the tetrakis (acetato)chloridodiruthenium(II, III) complex, *Angew. Chem. Int. Ed.* 53 (2014) 6172–6175.

[17] M. Kunzle, T. Eckert, T. Beck, Binary protein crystals for the assembly of inorganic nanoparticle superlattices, *J. Am. Chem. Soc.* 138 (2016) 12731–12734.

[18] S. Abe, T. Ueno, Design of protein crystals in the development of solid biomaterials, *RSC Adv.* 5 (2015) 21366–21375.

[19] T. Ueno, Porous protein crystals as reaction vessels, *Chem. Eur. J.* 19 (2013) 9096–9102.

[20] A.L. Margolin, M.A. Navia, Protein crystals as novel catalytic materials, *Angew. Chem. Int. Ed.* 40 (2001) 2204–2222.

[21] M. Guli, E.M. Lambert, M. Li, S. Mann, Template-directed synthesis of nanoplasmonic arrays by intracrystalline metalization of cross-linked lysozyme crystals, *Angew. Chem. Int. Ed.* 49 (2010) 520–523.

[22] H. Tabe, S. Abe, T. Hikage, S. Kitagawa, T. Ueno, Porous protein crystals as catalytic vessels for organometallic complexes, *Chem. Asian J.* 9 (2014) 1373–1378.

[23] S. Abe, M. Tsujimoto, K. Yoneda, M. Ohba, T. Hikage, M. Takano, S. Kitagawa, T. Ueno, Porous protein crystals as reaction vessels for controlling magnetic properties of nanoparticles, *Small* 8 (2012) 1314–1319.

[24] T. Koshiyama, M. Shirai, T. Hikage, H. Tabe, K. Tanaka, S. Kitagawa, T. Ueno, Post-crystal engineering of zinc-substituted myoglobin to construct a long-lived photo-induced charge-separation system, *Angew. Chem. Int. Ed.* 50 (2011) 4849–4852.

[25] M. Hansen, S. Troppmann, B. Konig, Artificial photosynthesis at dynamic self-assembled interfaces in water, *Chem. Eur. J.* 22 (2016) 58–72.

[26] S. Fukuzumi, Artificial photosynthetic systems for production of hydrogen, *Curr. Opin. Chem. Biol.* 25 (2015) 18–26.

[27] S. Berardi, S. Drouet, L. Francàs, C. Gimbert-Suriñach, M. Guttentag, C. Richmond, T. Stoll, A. Llobet, Molecular artificial photosynthesis, *Chem. Soc. Rev.* 43 (2014) 7501–7519.

[28] Z.J. Han, R. Eisenberg, Fuel from water: the photochemical generation of hydrogen from water, *Acc. Chem. Res.* 47 (2014) 2537–2544.

[29] Y.J. Yuan, Z.T. Yu, D.Q. Chen, Z.G. Zou, Metal-complex chromophores for solar hydrogen generation, *Chem. Soc. Rev.* 46 (2017) 603–631.

[30] C. Bachmann, B. Probst, M. Oberholzer, T. Fox, R. Alberto, Photocatalytic proton reduction with ruthenium and cobalt complexes immobilized on fumed reversed-phase silica, *Chem. Sci.* 7 (2016) 436–445.

[31] L. Duan, L. Wang, F. Li, F. Li, L. Sun, Highly efficient bioinspired molecular Ru water oxidation catalysts with negatively charged backbone ligands, *Acc. Chem. Res.* 48 (2015) 2084–2096.

[32] J. Li, Y. Wang, T. Zhou, H. Zhang, X. Sun, J. Tang, L. Zhang, A.M. Al-Enizi, Z. Yang, G. Zheng, Nanoparticle superlattices as efficient bifunctional electrocatalysts for water splitting, *J. Am. Chem. Soc.* 137 (2015) 14305–14312.

[33] L.Z. Wu, B. Chen, Z.J. Li, C.H. Tung, Enhancement of the efficiency of photocatalytic reduction of protons to hydrogen via molecular assembly, *Acc. Chem. Res.* 47 (2014) 2177–2185.

[34] D. Kim, D.R. Whang, S.Y. Park, Self-healing of molecular catalyst and photosensitizer on metal-organic framework: robust molecular system for photocatalytic H_2 evolution from water, *J. Am. Chem. Soc.* 138 (2016) 8698–8701.

[35] H. Zhou, F. Yu, Y. Huang, J. Sun, Z. Zhu, R.J. Nielsen, R. He, J. Bao, W.A. Goddard, S. Chen, Z. Ren, Efficient hydrogen evolution by ternary molybdenum sulfoselenide particles on self-standing porous nickel diselenide foam, *Nat. Commun.* 7 (2016) 12765.

[36] Y. Yamada, H. Tadokoro, M. Naqshbandi, J. Canning, M.J. Crossley, T. Suenobu, S. Fukuzumi, Nanofabrication of a solid-state, mesoporous nanoparticle composite for efficient photocatalytic hydrogen generation, *ChemPlusChem* 81 (2016) 521–525.

[37] Y. Yamada, H. Tadokoro, S. Fukuzumi, An effective preparation method of composite photocatalysts for hydrogen evolution using an organic photosensitizer and metalparticles assembled on alumina-silica, *Catal. Today* 278 (2016) 303–311.

[38] Y. Yamada, H. Tadokoro, S. Fukuzumi, Hybrid H_2 -evolution catalysts: *in situ* formation of H_2 -evolution catalysts from metal salts inside the mesopores of silica-alumina supporting an organic photosensitiser, *RSC Adv.* 3 (2013) 25677–25680.

[39] H. Kotani, T. Ono, K. Ohkubo, S. Fukuzumi, Efficient photocatalytic hydrogen evolution without an electron mediator using a simple electron donor-acceptor dyad, *Phys. Chem. Chem. Phys.* 9 (2007) 1487–1492.

[40] H. Tabe, T. Shimoi, M. Boudes, S. Abe, F. Coulibaly, S. Kitagawa, H. Mori, T. Ueno, Photoactivatable CO release from engineered protein crystals to modulate NF- κ B activation, *Chem. Commun.* 52 (2016) 4545–4548.

[41] M.C. Vaney, S. Maignan, M. Rieskauft, A. Ducruix, High-resolution structure (1.33 Å) of a HEW lysozyme tetragonal crystal grown in the APCF apparatus. Data and structural comparison with a crystal grown under microgravity from SpaceHab-01 mission, *Acta Crystallogr. D* 52 (1996) 505–517.

[42] H. Oki, Y. Matsuura, H. Komatsu, A.A. Chernov, Refined structure of orthorhombic lysozyme crystallized at high temperature: correlation between morphology and intermolecular contacts, *Acta Crystallogr. D* 55 (1999) 114–121.

[43] Z. Otwinowski, W. Minor, Processing of X-ray diffraction data collected in oscillation mode, *Method Enzymol.* 276 (1997) 307–326.

[44] A. Vagin, A. Teplyakov, *MOLREP*: an automated program for molecular replacement, *J. Appl. Crystallogr.* 30 (1997) 1022–1025.

[45] A.A. Vagin, R.A. Steiner, A.A. Lebedev, L. Potterton, S. McNicholas, F. Long, G.N. Mursudov, *REFMAC5* dictionary: organization of prior chemical knowledge and guidelines for its use, *Acta Crystallogr. D* 60 (2004) 2184–2195.

[46] E. Potterton, P. Briggs, M. Turkenburg, E. Dodson, A graphical user interface to the CCP4 program suite, *Acta Crystallogr. D* 59 (2003) 1131–1137.

[47] P. Emsley, K. Cowtan, *Coot*: model-building tools for molecular graphics, *Acta Crystallogr. D* 60 (2004) 2126–2132.

[48] S.C. Lovell, I.W. Davis, W.B. Arendall III, P.I.W. de Bakker, J.M. Word, M.G. Prisant, J.S. Richardson, D.C. Richardson, Structure validation by $\text{C}\alpha$ geometry: ϕ, ψ and $\text{C}\beta$ deviation, *Proteins: Struct. Funct. Genet.* 50 (2003) 437–450.

[49] A. Cvetkovic, A.J.J. Straathof, R. Krishna, L.A.M. van der Wielen, Adsorption of xanthene dyes by lysozyme crystals, *Langmuir* 21 (2005) 1475–1480.

[50] S.W. Tanley, L.V. Starkey, L. Lamplough, S. Kaenket, J.R. Helliwell, The binding of platinum hexahalides (Cl, Br and I) to hen egg-white lysozyme and the chemical transformation of the PtI_6 octahedral complex to a PtI_3 moiety bound to His15, *Acta Crystallogr. F* 70 (2014) 1132–1134.

[51] L. Messori, T. Marzo, C. Gabbiani, A.A. Valdes, A.G. Quiroga, A. Merlin, Peculiar features in the crystal structure of the adduct formed between *cis*- $\text{PtI}_2(\text{NH}_3)_2$ and hen egg white lysozyme, *Inorg. Chem.* 52 (2013) 13827–13829.

[52] <http://www.pymol.org/>, (Accessed 06, December 2017).

[53] X. Zhang, Z. Jin, Y. Li, S. Li, G. Lu, Efficient photocatalytic hydrogen evolution from water without an electron mediator over Pt-rose bengal catalysts, *J. Phys. Chem. C* 113 (2009) 2630–2635.

[54] P.D. Sun, S. Radaev, M. Kattah, Generating isomorphous heavy-atom derivatives by a quick-soak method part I: test cases, *Acta Crystallogr. D* 58 (2002) 1092–1098.